AIP | Applied Physics Letters

Interface engineering for efficient fullerene-free organic solar cells

Ravichandran Shivanna, Sridhar Rajaram, and K. S. Narayan

Citation: Applied Physics Letters **106**, 123301 (2015); doi: 10.1063/1.4916216
View online: http://dx.doi.org/10.1063/1.4916216
View Table of Contents: http://scitation.aip.org/content/aip/journal/apl/106/12?ver=pdfcov
Published by the AIP Publishing

Interface engineering for efficient fullerene-free organic solar cells

Ravichandran Shivanna,[1] Sridhar Rajaram,[2,a)] and K. S. Narayan[1,a)]
[1]*Chemistry and Physics of Materials Unit, Jawaharlal Nehru Centre for Advanced Scientific Research, Bangalore 560064, India*
[2]*International Centre for Materials Science, Jawaharlal Nehru Centre for Advanced Scientific Research, Bangalore 560064, India*

(Received 22 January 2015; accepted 12 March 2015; published online 23 March 2015)

We demonstrate the role of zinc oxide (ZnO) morphology and addition of an acceptor interlayer to achieve high efficiency fullerene-free bulk heterojunction inverted organic solar cells. Nanopatterning of the ZnO buffer layer enhances the effective light absorption in the active layer, and the insertion of a twisted perylene acceptor layer planarizes and decreases the electron extraction barrier. Along with an increase in current homogeneity, the reduced work function difference and selective transport of electrons prevent the accumulation of charges and decrease the electron-hole recombination at the interface. These factors enable an overall increase of efficiency to 4.6%, which is significant for a fullerene-free solution-processed organic solar cell. © *2015 AIP Publishing LLC*. [http://dx.doi.org/10.1063/1.4916216]

Bulk heterojunction (BHJ) organic photovoltaic (OPV) technology is a potential alternative due to roll-to-roll processability, cost-effectiveness, and ease of installation.[1,2] Power conversion efficiency (PCE) of this technology has gradually improved to around ~10%.[3,4] Most of the efforts towards the enhancement of PCE of OPVs have been towards the design and synthesis of new donor polymers with improved optical absorption extending to near IR regime and increased hole mobilites. In contrast, relatively less effort has been directed towards alternate acceptors. Hence, till date, the most common electron acceptor materials in all these high efficient solar cells are fullerene derivatives.[5,6] The dominance of fullerene derivatives as electron acceptors is due to their high electron mobility, high electron affinity, and isotropic charge transfer. However, the use of fullerene based OPVs has important drawbacks including low absorption in the visible region, elaborate synthetic procedure, and limited tunability of energy levels.[7,8] Tang reported the first organic photovoltaic devices using perylene as the electron acceptor,[9] however, the efficiency was limited by bulk nanomorphology. In this regard, considerable progress has been made in the recent years in developing new electron acceptors.[10,11] Thereafter, fullerene-free solar cells and specifically perylene derivatives have seen a drastic improvement in the PCE higher than 6%.[12–21] Recently, we demonstrated that disrupting the planarity of the perylene by perpendicularly orienting two units reduces the co-facial stacking and hence improved the blend morphology. This resulted in an order of magnitude increase in the short circuit current density in OPVs made from this acceptor material.[12] We further analyzed the dynamics of charge generation and transport using ultrafast transient absorption spectroscopy. It was concluded that the charge generation magnitude in the twisted perylene (TP) acceptor blend system is comparable to that of fullerene blends.[13] The challenge of charge transport and extraction in TP blends needed further optimization to achieve a high PCE. Since the TP molecules are fundamentally different from fullerene based acceptors in terms of bulk organization, phase distribution, and electrode-interface formation, conventional approaches utilized for fullerene blends may not be directly applicable. In this report, we address these issues and present a combination of strategies involving a patterned ZnO layer and an acceptor interlayer to enhance the PCE of the TP based solar cell devices.

The spontaneous formation of nano-structures in solution deposited electron-extracting metal oxide layer was shown to enhance optical absorption due to scattering at the active layer interface in inverted OPVs.[22–24] The sol-gel based ZnO films of controlled thickness exhibited interesting, spontaneous formation of wrinkles upon annealing.[25] In addition to the functionality of selectively extracting electrons, ZnO wrinkles provided appropriate texturing and effectively increased the optical path length. However, the wrinkling engenders current inhomogeneity. This was compensated by surface modification.[23,26,27] In this report, the wrinkled ZnO surface is modified by inserting an ultrathin electron conducting TP layer prior to depositing the active layer. This procedure leads to reduced bimolecular recombination at the electron extracting interface, which is evident from conducting and surface potential mapping measurements.

Atomic force microscopy (AFM) images of ZnO sol-gel films spin coated at different speed on top of ITO coated glass substrate are illustrated in Figs. 1(a)–1(e). The top and bottom row represent the height and corresponding phase image, respectively, obtained from a high-resolution AFM (JPK Instruments, Inc., Germany) system. The images exhibit isotropic wrinkle patterns with characteristic spacing (λ), fractal length (L_f), and root mean squared (RMS) surface roughness (σ_{rms}). The wrinkle formation in a thin film is attributed to the deformation introduced from factors leading to surface instability.[28] For sol-gel based thin films, the compressive stress is generated during the evaporation of solvent due to the difference in the thermal expansion coefficient between the film and the substrate.[29] This compressive stress induces a volumetric strain in the film leading to nucleation of wrinkles.[30] Further increase in the temperature above the boiling

a)Electronic addresses: rajaram@jncasr.ac.in and narayan@jncasr.ac.in

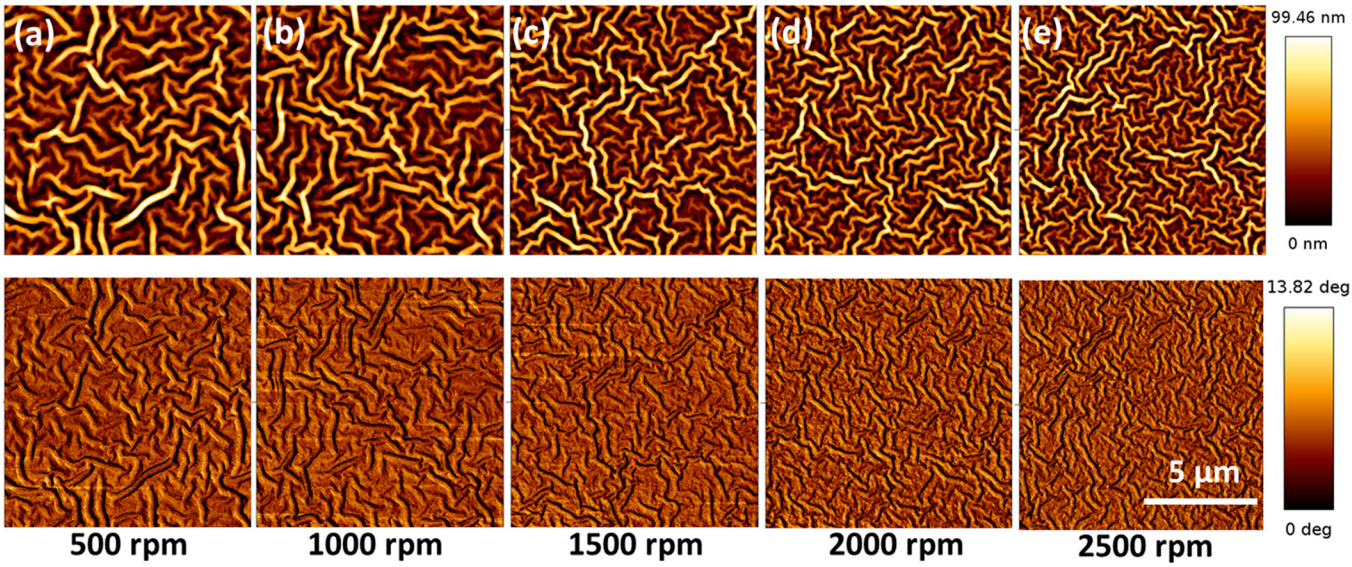

FIG. 1. Wrinkling of ZnO Sol gel films upon annealing. Change in the wavelength and fractal length of the wrinkles with different film thickness varied by spin coating at different speed (a)–(e). Top row is the AFM height image and bottom row shows the corresponding phase image.

point of the solvent increases the volumetric strain in the film. This process leads to bending of the gelated film and finally results in the formation of a network of wrinkles.[30] The characteristics of wrinkles are strongly dependent on film thickness [$\lambda \approx (d)^{0.75}$] and annealing conditions.[29] The wrinkle density and surface roughness of the film also increases with annealing time while maintaining the characteristic "λ." In our procedure, ZnO sol-gel precursor was prepared by dissolving 314 mg of zinc acetate dihydrate [$Zn(CH_3COO)_2.2H_2O$] (Sigma-Aldrich) in 314 ml of 2-methoxyethanol (Sigma-Aldrich) and 86 μl of ethanolamine as stabilizer. The solution was stirred for 1 h at 65 °C and left for 3 h to form a gel. The sol-gel precursor was spin coated at different speeds, annealed with ramp rate of 5 °C/min till 150 °C and kept at 150 °C for 2 h in air. Fig. 1 represents the formation of wrinkles of ZnO films with different λ, L_f, and σ_{rms} spun at different speed from the same precursor annealed at similar condition. The L_f decreases from ~1.4 μm to ~0.6 μm and λ decreases from ~800 nm to ~200 nm for the films coated at 500 rpm and 2500 rpm, respectively.[30] Corresponding phase images show more uniform distribution exhibiting complete formation of ZnO.

Blend films consisting of PBDTTT-CT electron donor and TP electron acceptor (Fig. 2(c), inset) in a 1:1 ratio by weight were spin coated (12 mg/ml solution concentration in anhydrous chlorobenzene inside a nitrogen filled glovebox at 1000 rpm) on the ZnO layer. This procedure of spin coating resulted in an active layer of ~100 nm film thickness on a planar surface, which was optimum for efficient charge generation in BHJ systems.[13] Two important factors that have to be considered in depositing the active layer on nanostructured films were surface wettability and the pinhole-free surface coverage of active layer.[31] Increased surface roughness generally leads to pinhole effects resulting in overall

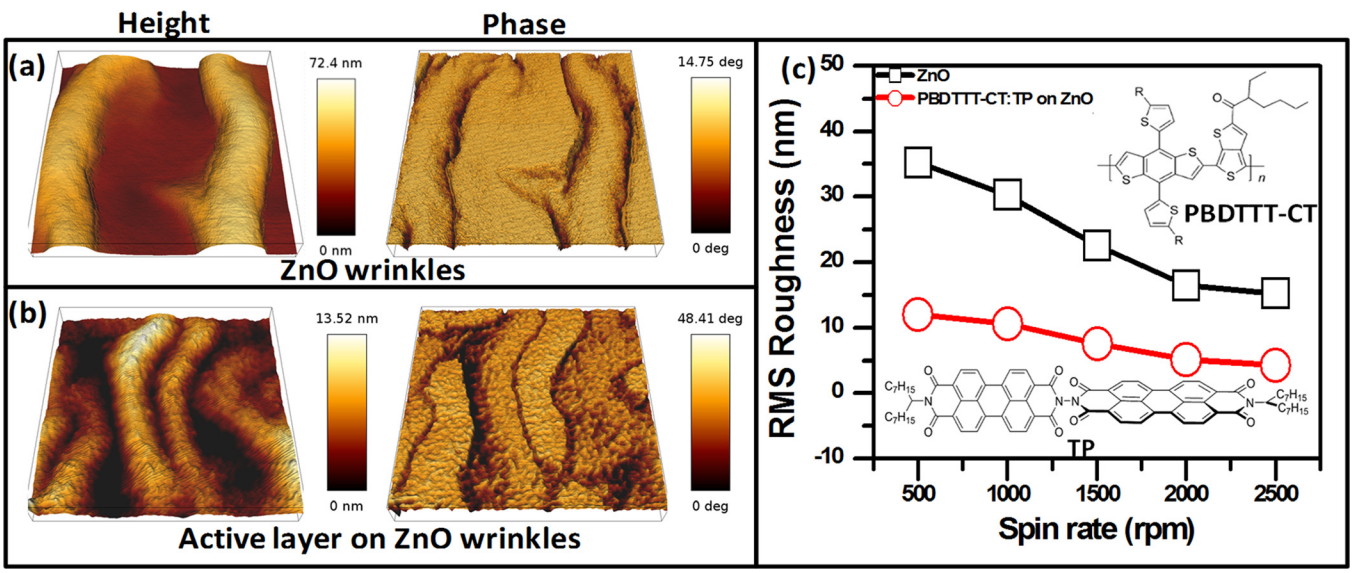

FIG. 2. Wetting of ZnO wrinkles with PBDTTT-CT:TP active layer. (a) AFM height and phase image showing the features of bare wrinkles, (b) AFM height and phase image exhibiting complete wetting of ZnO surface with PBDTTT-CT:TP BHJ, and (c) RMS roughness of the surface with and without PBDTTT-CT:TP on ZnO at different rpm films. Area of the 3D images is 1 μm × 1 μm. Inset in (c) shows the chemical structure of PBDTTT-CT and TP.

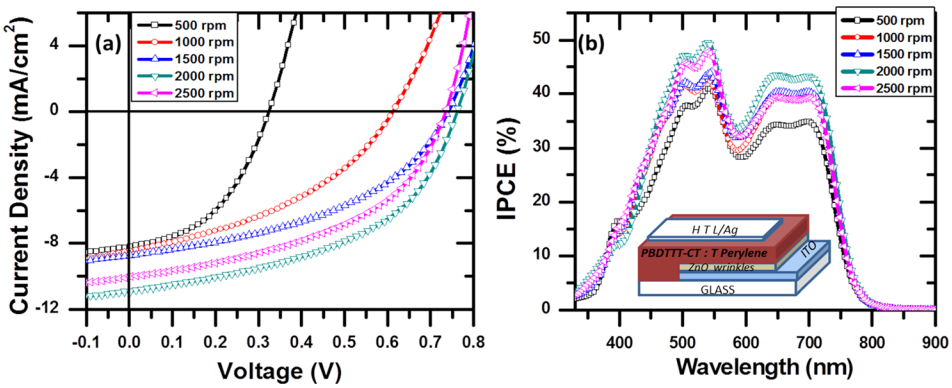

FIG. 3. (a) J-V curves of solar cells of 1:1 ratio PBDTTT-CT:TP BHJ on ZnO wrinkle surface formed by spin coating at different rpms. (b) Corresponding IPCE of solar cells. Inset in (b) shows the device architecture.

reduction of PCE, open circuit voltage, and fill factor (FF). Figs. 2(a) and 2(b) represent the surface morphology of ZnO and PBDTTT-CT:TP/ZnO films. Comparison of height and phase images between the films clearly demonstrates the decrease in the peak-to-valley roughness and areal coverage. This trend is established throughout the surface as shown in the large area scan.[30] Phase image exhibits increased phase difference on the PBDTTT-CT:TP/ZnO surface due to the donor-acceptor components in the BHJ. σ_{rms} reduces from ~35 nm to ~12 nm for the ZnO film coated at 500 rpm without and with active layer, respectively. Fig. 2(c) represents the monotonic decrease of σ_{rms} with increase in spin rate for both the films.

The fabrication of inverted solar cells was completed by thermal evaporation of hole transport layer MoOx (~11 nm) followed by deposition of Ag (~100 nm) using a shadow mask at a base pressure of 10^{-6} mbar. The current density(J)-voltage(V) characteristics of solar cells fabricated by spin coating ZnO films at different rate are represented in Fig. 3(a). The results are tabulated in Table I. When the spin speed for depositing ZnO was increased from 500 to 2000 rpm, then the short circuit current density (J_{sc}) increases from 8.15 to 10.02 mA/cm^2 and the open circuit voltage increases (V_{oc}) from 0.32 to 0.73 V. The maximum PCE of 4.02%, $J_{sc} = 10.9$ mA/cm^2, $V_{oc} = 0.76$, and FF = 48.4% was achieved for ZnO layer coated at 2000 rpm. In comparison to the planar ZnO layer, the nanostructured ZnO layer offers a higher interfacial area, which enables charge extraction process. Fig. 3(b) shows the incident photon to current conversion efficiency (IPCE) of these devices. The bimodal absorption of blend components leads to efficient generation of charges over the entire visible spectrum (400–800 nm) with maxima at 540 nm for all the devices. Maximum IPCE of ~50% at 540 nm was obtained for the device with 2000 rpm ZnO layer. The calculated J_{sc} from the IPCE curve correlates with the measured device J_{sc} for all the films. The inset of Fig. 3(b) shows the schematic of a complete device consisting of Glass/ITO/ZnO/PBDTTT-CT:TP/MoOx/Ag. The absorption of ZnO/PBDTTT-CT:TP films with different ZnO rpm rates exhibits increased contribution of ZnO absorption below 400 nm.[30] However, the IPCE does not show significant photocurrent below 400 nm in the device. This clearly indicates that ZnO has minimal contribution to carrier photogeneration. Increased PCE is mainly assisted by efficient electron extraction at the ZnO/PBDTTT-CT:TP interface. Further, variation of ZnO thickness varies the optical field profile inside the BHJ. This is evident from the normalized IPCE spectra.[30]

TABLE I. J-V characteristics of solar cells on ZnO wrinkle of different thickness.

Speed (rpm)	J_{sc} (mA/cm^2)	V_{oc} (V)	FF (%)	η (%)[a]
500	8.15 ± 0.2	0.322 ± 0.010	45.62 ± 0.7	1.20 ± 0.12 (1.34)
1000	8.45 ± 0.4	0.615 ± 0.015	40.24 ± 1.0	2.07 ± 0.18 (2.12)
1500	8.69 ± 0.3	0.739 ± 0.009	44.30 ± 0.6	2.84 ± 0.07 (2.93)
2000	10.85 ± 0.1	0.760 ± 0.005	48.41 ± 0.2	3.99 ± 0.03 (4.02)
2500	10.02 ± 0.1	0.733 ± 0.006	46.56 ± 0.3	3.42 ± 0.06 (3.53)

[a]Number in the brackets show highest efficiency devices.

To further optimize the cells, a thin layer of electron acceptor was introduced between the ZnO wrinkle surface and the photo-active layer. Cho *et al.*[27] have reported 16% increase in PCE by adding $PC_{61}BM$ interlayer between ZnO and BHJ. The insertion of additional $PC_{61}BM$ interlayer enhanced current homogeneity and lowered charge accumulation at the interface. Here, we utilize the ultrathin layer of TP as electron extractor between ZnO wrinkle surface and PBDTTT-CT:TP active layer. TP solution of 1 mg/ml concentration in anhydrous chlorobenzene was spin coated at 1000 rpm for 60 s on top of ZnO wrinkles. The films were annealed at 100 °C for 5 min. Just before coating the active blend layer, an orthogonal-solvent (ethanol) was spin coated at 1000 rpm for 5 s to avoid the re-dispersal of the thin TP layer upon introduction of the blend solution. Conducting AFM imaging was used to follow the electron extracting homogeneity of TP interlayer on the ZnO wrinkle surface, as shown in Figures 4(a) and 4(b), with a bias between ITO and Pt/Cr coated CAFM tip. Wrinkled ZnO surface without TP interlayer shows inhomogeneous current mapping. The current values exhibit maxima in the trenches and minima at the ridges. Under similar bias conditions, the ZnO surface with TP interlayer display more homogenous current mapping. In effect, the additional TP layer increases the uniformity of electron extraction at the electrode:active-layer interface. Further, the solar cell fabrication was completed by evaporating MoOx and Ag on top of the active layer. Fig. 4(c) represents the J-V characteristics of devices with and without the TP interlayer. The cell with TP interlayer shows an enhanced PCE of 4.6%, with $J_{sc} = 11.9$ mA/cm^2, $V_{oc} = 0.76$ V, and FF = 50.3%. Adequate number of devices fabricated to arrive at a statistics, necessary to affirm the

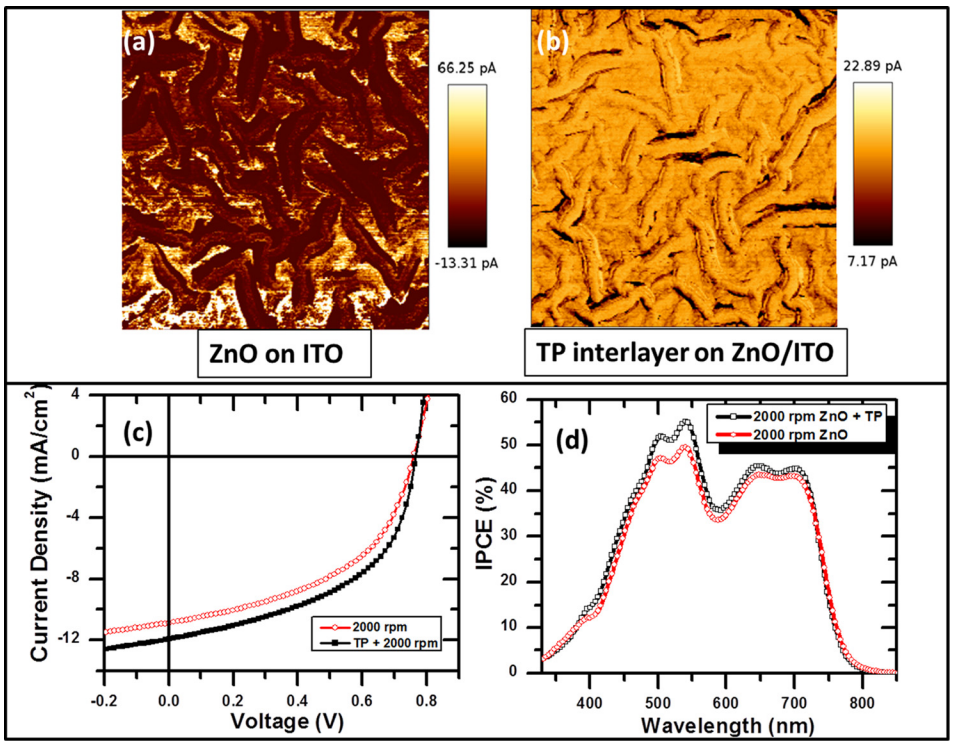

FIG. 4. (a) CAFM of bare ZnO surface and (b) Zno surface coated with TP interlayer. (c) J-V curves of solar cells of 1:1 ratio PBDTTT-CT:TP BHJ on ZnO surface with and without TP interlayer. (c) Corresponding IPCE of solar cells showing maximum of 55% at $\lambda \approx 540$ nm. Scale bar represents the current measured at 8 V bias w.r.t Pt/Cr coated tip.

trend. This represents a 15% increase in PCE when compared to devices without TP interlayer. This high PCE places the device among the group of highly efficient fullerene-free organic BHJ solar cells. The J-V curve clearly indicates that the enhanced PCE with additional TP layer is due to the increase in J_{sc} when compared to devices without TP interlayer. Increased J_{sc} is attributed to increased current homogeneity at the ZnO and the active layer interface.[32] Reduced bimolecular recombination of photogenerated electrons and holes at the charge extracting interface assists in increasing overall charge extraction efficiency. Fig. 4(d) shows the IPCE spectra of devices with and without TP interlayer. Devices with TP interlayer exhibit overall increase in the IPCE spectrum with maximum of ~55% at ~540 nm. This is further evident from the increased J_{sc} in the J-V characteristics. Additionally, J_{sc} estimated from IPCE correlates with the measured J_{sc} from the J-V curve. In addition, Kelvin probe force microscopy (KPFM) was carried out to map the surface potential of ZnO with and without TP interlayer.[30] Surface potential with respect to Pt/Cr coated AFM tip shows reduced potential between ZnO and ZnO + TP layers. This implies that ZnO with TP interlayer effectively reduces the work function of the electrode leading to efficient extraction of electrons. The overall increase in IPCE spectrum and reduced work function from KPFM data suggests that the additional TP interlayer essentially contributes to the charge extraction process along with relatively increased photocharge generation from the TP absorption. In our previous studies,[13] it was shown that the charge generation efficiency of TP blends is comparable with $PC_{70}BM$ blends. However, the device efficiency was limited by the charge transport through the bulk. In the present study, we demonstrate that the charge extraction efficiency can be improved by utilizing an additional TP layer between ZnO and active layer. A 15% improvement in PCE is observed compared to devices without the additional TP layer. This improvement follows the trend observed in fullerene based cells, where an additional $PC_{60}BM$ layer was introduced to improve the charge extraction[27] and PCE by 16%. These set of observations indicate that, in general, the additional pristine acceptor layer can enhance PCE by improving electron extraction.

In conclusion, an overall increase of >40% in PCE in TP based BHJs was achieved utilizing nanostructured ZnO wrinkles and insertion of a TP electron acceptor interlayer. The features of the ZnO wrinkles were controlled by spin coating the sol-gel at different speeds. The wrinkles enhanced the light-harvesting efficiency of the active layer by acting as light scattering centers along with increased surface area. Good surface coverage was obtained by spin coating active layer on top of ZnO wrinkles. The devices with PBDTTT-CT:TP photoactive layer exhibited enhanced performance with PCE as high as 4%. IPCE spectra of these devices concluded that the ZnO wrinkles contribute more towards the charge extraction property than photogeneration of charge carriers. The cells with additional TP interlayer introduced between the ZnO wrinkles and the active layer exhibited superior performance. The devices exhibited a PCE of 4.6%, which is among the high efficient fullerene free-organic BHJ solar cells. IPCE reached a maximum of 55% at 540 nm. The 15% increase in PCE is attributed to increased current homogeneity at the ZnO wrinkle and photoactive layer interface as measured by CAFM. In addition, KPFM showed a decrease in work function of the ZnO surface containing TP interlayer. We attribute the enhanced performance of the device to efficient extraction by reduced bimolecular recombination of photogenerated electrons and holes at the ZnO wrinkles and photo active layer interface. Further refinements in the present approach can possibly lead to device performances comparable to fullerene based BHJs.

We acknowledge Indo-UK APEX project and Sunil Kumar for synthesis of TP.

[1]R. Søndergaard, M. Hösel, D. Angmo, T. T. Larsen-Olsen, and F. C. Krebs, Mater. Today **15**(1–2), 36 (2012).
[2]T. M. Clarke and J. R. Durrant, Chem. Rev. **110**(11), 6736 (2010).
[3]Z. He, C. Zhong, S. Su, M. Xu, H. Wu, and Y. Cao, Nat. Photonics **6**(9), 591 (2012).
[4]J. You, L. Dou, K. Yoshimura, T. Kato, K. Ohya, T. Moriarty, K. Emery, C.-C. Chen, J. Gao, G. Li, and Y. Yang, Nat. Commun. **4**, 1446 (2013).
[5]J. C. Hummelen, B. W. Knight, F. LePeq, F. Wudl, J. Yao, and C. L. Wilkins, J. Org. Chem. **60**(3), 532 (1995).
[6]M. M. Wienk, J. M. Kroon, W. J. H. Verhees, J. Knol, J. C. Hummelen, P. A. van Hal, and R. A. J. Janssen, Angew. Chem. Int. Ed. **42**(29), 3371 (2003).
[7]M. C. Scharber, D. Mühlbacher, M. Koppe, P. Denk, C. Waldauf, A. J. Heeger, and C. J. Brabec, Adv. Mater. **18**(6), 789 (2006).
[8]E. Bundgaard and F. C. Krebs, Sol. Energy Mater. Sol. Cells **91**(11), 954 (2007).
[9]C. W. Tang, Appl. Phys. Lett. **48**(2), 183 (1986).
[10]Y. Lin and X. Zhan, Mater. Horiz. **1**(5), 470 (2014).
[11]X. Guo, A. Facchetti, and T. J. Marks, Chem. Rev. **114**(18), 8943 (2014).
[12]S. Rajaram, R. Shivanna, S. Kumar Kandappa, and K. S. Narayan, J. Phys. Chem. Lett. **3**(17), 2405 (2012).
[13]R. Shivanna, S. Shoaee, S. Dimitrov, S. Kumar Kandappa, S. Rajaram, J. R. Durrant, and K. S. Narayan, Energy Environ. Sci. **7**(1), 435 (2014).
[14]R. Singh, E. Aluicio-Sarduy, Z. Kan, T. Ye, R. C. I. MacKenzie, and P. E. Keivanidis, J. Mater. Chem. A **2**(35), 14348 (2014).
[15]P. E. Hartnett, A. Timalsina, H. S. S. Ramakrishna Matte, N. Zhou, X. Guo, W. Zhao, A. Facchetti, R. P. H. Chang, M. C. Hersam, M. R. Wasielewski, and T. J. Marks, J. Am. Chem. Soc. **136**(46), 16345 (2014).
[16]Y. Zhong, M. T. Trinh, R. Chen, W. Wang, P. P. Khlyabich, B. Kumar, Q. Xu, C.-Y. Nam, M. Y. Sfeir, C. Black, M. L. Steigerwald, Y.-L. Loo, S. Xiao, F. Ng, X. Y. Zhu, and C. Nuckolls, J. Am. Chem. Soc. **136**(43), 15215 (2014).
[17]Y. Zang, C.-Z. Li, C.-C. Chueh, S. T. Williams, W. Jiang, Z.-H. Wang, J.-S. Yu, and A. K. Y. Jen, Adv. Mater. **26**(32), 5708 (2014).
[18]D. Mori, H. Benten, I. Okada, H. Ohkita, and S. Ito, Energy Environ. Sci. **7**(9), 2939 (2014).
[19]X. Zhang, C. Zhan, and J. Yao, Chem. Mater. **27**(1), 166 (2014).
[20]Y. Lin, Z.-G. Zhang, H. Bai, J. Wang, Y. Yao, Y. Li, D. Zhu, and X. Zhan, Energy Environ. Sci. **8**, 610–616 (2015).
[21]Y. Lin, J. Wang, Z.-G. Zhang, H. Bai, Y. Li, D. Zhu, and X. Zhan, Adv. Mater. **27**, 1170 (2015).
[22]D. C. Lim, K.-D. Kim, S.-Y. Park, E. Mi Hong, H. Ook Seo, J. H. Lim, K. H. Lee, Y. Jeong, C. Song, E. Lee, Y. Dok Kim, and S. Cho, Energy Environ. Sci. **5**(12), 9803 (2012).
[23]C.-H. Hsieh, Y.-J. Cheng, P.-J. Li, C.-H. Chen, M. Dubosc, R.-M. Liang, and C.-S. Hsu, J. Am. Chem. Soc. **132**(13), 4887 (2010).
[24]Y.-J. Cheng, C.-H. Hsieh, Y. He, C.-S. Hsu, and Y. Li, J. Am. Chem. Soc. **132**(49), 17381 (2010).
[25]D. C. Lim, W. H. Shim, K.-D. Kim, H. Ook Seo, J.-H. Lim, Y. Jeong, Y. Dok Kim, and K. H. Lee, Sol. Energy Mater. Sol. Cells **95**(11), 3036 (2011).
[26]K.-D. Kim, D. C. Lim, J. Hu, J.-D. Kwon, M.-G. Jeong, H. Ook Seo, J. Y. Lee, K.-Y. Jang, J.-H. Lim, K. H. Lee, Y. Jeong, Y. D. Kim, and S. Cho, ACS Appl. Mater. Interfaces **5**(17), 8718 (2013).
[27]S. Cho, K.-D. Kim, J. Heo, J. Y. Lee, G. Cha, B. Y. Seo, Y. D. Kim, Y. S. Kim, S.-Y. Choi, and D. C. Lim, Sci. Rep. **4**, 4306 (2014).
[28]N. Bowden, S. Brittain, A. G. Evans, J. W. Hutchinson, and G. M. Whitesides, Nature **393**(6681), 146 (1998).
[29]S. J. Kwon, J.-H. Park, and J.-G. Park, Phys. Rev. E **71**(1), 011604 (2005).
[30]See supplementary material at http://dx.doi.org/10.1063/1.4916216 for AFM images, absorbance, norm IPCE, and KPFM data.
[31]S. Mukhopadhyay, A. J. Das, and K. S. Narayan, J. Phys. Chem. Lett. **4**(1), 161 (2012).
[32]D. Gupta, M. Bag, and K. S. Narayan, Appl. Phys. Lett. **92**(9), 093301 (2008).